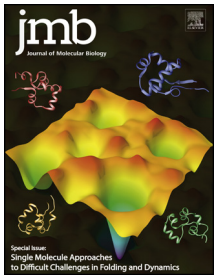

Soft Interactions with Model Crowders and Non-canonical Interactions with Cellular Proteins Stabilize RNA Folding

May Daher [1,2], Julia R. Widom [1,2], Wendy Tay [1,3] and Nils G. Walter [1,2]

*1 - **Single Molecule Analysis Group,** Department of Chemistry, University of Michigan, Ann Arbor, MI 48109-1055, USA*
*2 - **Center for RNA Biomedicine,** University of Michigan, Ann Arbor, MI 48109-1055, USA*
*3 - **Program in Chemical Biology,** University of Michigan, Ann Arbor, MI 48109-1055, USA*

***Correspondence to Nils G. Walter:** Single Molecule Analysis Group, Department of Chemistry, University of Michigan, Ann Arbor, MI 48109-1055, USA. nwalter@umich.edu*
https://doi.org/10.1016/j.jmb.2017.10.030
Edited by Philip C. Bevilacqua

Abstract

Living cells contain diverse biopolymers, creating a heterogeneous crowding environment, the impact of which on RNA folding is poorly understood. Here, we have used single-molecule fluorescence resonance energy transfer to monitor tertiary structure formation of the hairpin ribozyme as a model to probe the effects of polyethylene glycol and yeast cell extract as crowding agents. As expected, polyethylene glycol stabilizes the docked, catalytically active state of the ribozyme, in part through excluded volume effects; unexpectedly, we found evidence that it additionally displays soft, non-specific interactions with the ribozyme. Yeast extract has a profound effect on folding at protein concentrations 1000-fold lower than found intracellularly, suggesting the dominance of specific interactions over volume exclusion. Gel shift assays and affinity pull-down followed by mass spectrometry identified numerous non-canonical RNA-binding proteins that stabilize ribozyme folding; the apparent chaperoning activity of these ubiquitous proteins significantly compensates for the low-counterion environment of the cell.

Introduction

The cell interior is packed with different types of biopolymers that occupy 20%–40% of the total cellular volume [1–4]. This packing, denoted "macromolecular crowding," decreases the volume of the solvent available, leading to excluded volume (EV) effects on biomolecules and biomolecular interactions that lately have been studied extensively *in vitro*. Complementary studies under cellular environments have revealed significant consequences of the EV effect on cell physiology and different cellular processes including molecular associations, cellular structure and intracellular signaling [5].

Studies assessing RNA in the presence of macromolecular crowding have revealed significant insights into RNA folding, function and thermodynamics [6,7]. Computational studies have shown that more compact structures of RNA are favored in crowded conditions [8,9]. Small-angle X-ray scattering, single-molecule fluorescence resonance energy transfer (smFRET) and biochemical studies revealed an enhancement of the biochemical function of numerous catalytic RNAs when active folding was induced by the presence of a high-molecular-weight model crowder. For instance, polyethylene glycol (PEG) was recently reported to enhance folding and accelerate the cleavage activity of two small catalytical RNAs, the hairpin ribozyme [10] and the hammerhead ribozyme [6,11–13], as well as of large ribozymes [14,15]. The cellular environment can be further mimicked through compartmentalization. In particular, it was shown that upon partitioning of a ribozyme into a dextran-rich aqueous phase, its rate of cleavage is enhanced by ~70-fold [16]. However, studies addressing the influence of a more complex, cell-like milieu on RNA structure and function under controlled conditions are limited and suggest that the effects of the cellular environment on RNA folding are not be recapitulated by the simple addition of inert crowding agents [7].

The intracellular environment is distinguished from typical *in vitro* models of crowding by the presence of

different types of biomolecules such as polysaccharides, proteins, nucleic acids and other co-solutes of different sizes, shapes and charges. Through volume exclusion as well as specific and nonspecific interactions, these biomolecules may exert diverse influences on RNA folding and many other cellular processes [17–21]. For example, the highly crowded environment is thought to induce nonspecific attractive and repulsive interactions among macromolecules [21,22] and proteins are known to bind nonspecifically to RNA albeit at a lower affinity than those of specific interactions [23,24]. These numerous interactions can potentially affect a macromolecule's structure, dynamics and function [21,25]. The current lack of a full understanding of these effects is one reason why emerging *in vivo* RNA structure probing data remain challenging to interpret [26–29]. Therefore, it becomes ever more critical to examine the folding processes of RNA model systems in a controlled cell-like milieu.

Here, we used the hairpin ribozyme to investigate the tertiary structure folding dynamics of an RNA model system under controlled cell-mimicking crowding conditions (Fig. 1). Found in the tobacco ring-spot virus satellite RNA, this ribozyme is involved in the replication of the viroid through backbone self-cleavage and -ligation [30–32]. The ribozyme adopts two well-defined conformations, docked (folded, catalytically active) and undocked (unfolded, inactive), that can be conveniently monitored by smFRET (Fig. 1a,b). A stable docked (high-FRET) conformation is observed *in vitro* in the presence of high concentrations of divalent metal ions [32–34]. Single-molecule studies on the two-way junction hairpin ribozyme have broadly dissected the folding dynamics and cleavage mechanism in dilute solutions [32–35].

Here, we investigate the conformational changes of the ribozyme in the presence of the model crowding agent PEG (8-kDa molecular weight), or in the presence of yeast whole cell extract (WCE). There is strong biological relevance to the folding of viral ribozymes under eukaryotic cellular conditions, for which yeast WCE is a convenient model. For example, there has been progress in using these small catalytic RNAs to inhibit tumorigenesis and to treat acquired immunodeficiency syndrome as well as other diseases [36–39]. Such applications face numerous challenges, however, including nucleolytic degradation and other unintended effects resulting from interactions with cellular proteins. The latter is a major focus of the study we present here.

Consistent with prior studies [6,10], our results indicate that PEG stabilizes the native fold of the ribozyme. In contrast to previous studies on a smaller RNA species [6], however, we found that this effect occurs at lower concentrations of PEG than predicted from a hard-sphere interaction model, and that the trend is better fit by a model invoking weak binding of PEG to the ribozyme. This implies that soft, non-specific interactions with PEG, rather than purely EV effects, drive folding at low concentrations. We further discovered that at protein concentrations of WCE 1000-fold lower than those found in the cell (corresponding to mass concentrations >10-fold lower than those effective for PEG), the folded state of the hairpin ribozyme is significantly stabilized. Affinity pull-down assays followed by mass spectrometry identified specific and non-specific RNA-binding proteins that appear responsible for this stabilization, including non-canonical RNA-binding proteins from among those recently found to bear cryptic RNA binding sites [40,41]. Such abundant, relatively nonspecific protein interactions are likely to exert significant influence over RNA structure and folding *in vivo*.

Results and Discussion

PEG stabilizes the folded state of the hairpin ribozyme, in part through soft interactions

In this study, we first investigated the impact of PEG with an average “”molecular weight of 8 kDa (PEG8000), a neutral, highly water soluble, chemically inert linear polymer and model crowder, on the folding thermodynamics and kinetics of a minimal two-way junction hairpin ribozyme with a non-cleavable substrate strand (Fig. 1a) that has been extensively characterized by smFRET in dilute solution [32–35]. We first investigated this RNA in the presence of varying concentrations of PEG in standard reaction

Fig. 1. Effect of PEG8000 on the folding dynamics of the hairpin ribozyme. (a) Schematic representation of the secondary structure, loop A–loop B docking interaction (anchored by a G:C base pair in red), and sequence of the two-way junction hairpin ribozyme composed of strands RzA, RzB and, in lower-case letters, substrate. A biotin on RzB was used to immobilize the RNA on a slide. (b) The hairpin ribozyme was immobilized on a PEGylated-quartz slide via a biotin–streptavidin linkage and imaged by TIRFM within a surface-specific evanescent field (green shade). (c) FRET probability histograms built from N molecules each, at varying PEG concentrations. Two major FRET states were observed and fitted with Gaussian distributions (green, low-FRET state; red, high-FRET state). (d) Representative time trajectories of dynamic single molecules at 0, 80 or 200 mg/mL PEG concentration. Idealizations generated by Hidden Markov Modeling are shown in cyan. (e) The fraction of docked states as a function of PEG concentration (f_d), which saturated at a value of 0.86, was fitted with a non-cooperative binding isotherm (black line), revealing PEG_{50} = 54 ± 10 mg/mL. (f) Stabilization of the docked conformation at different PEG conditions relative to the absence of crowder.

buffer [32–34] [50 mM Tris–HCl (pH 7.5) and 12 mM $MgCl_2$]. We placed donor and acceptor fluorophores on the ribozyme (Fig. 1a) in a way that allowed us to observe the undocked and docked conformations as low- and high-FRET states, respectively, by total internal reflection fluorescence microscopy (TIRFM; Fig. 1b). The resulting FRET probability distribution histograms for at least 100 molecules per condition

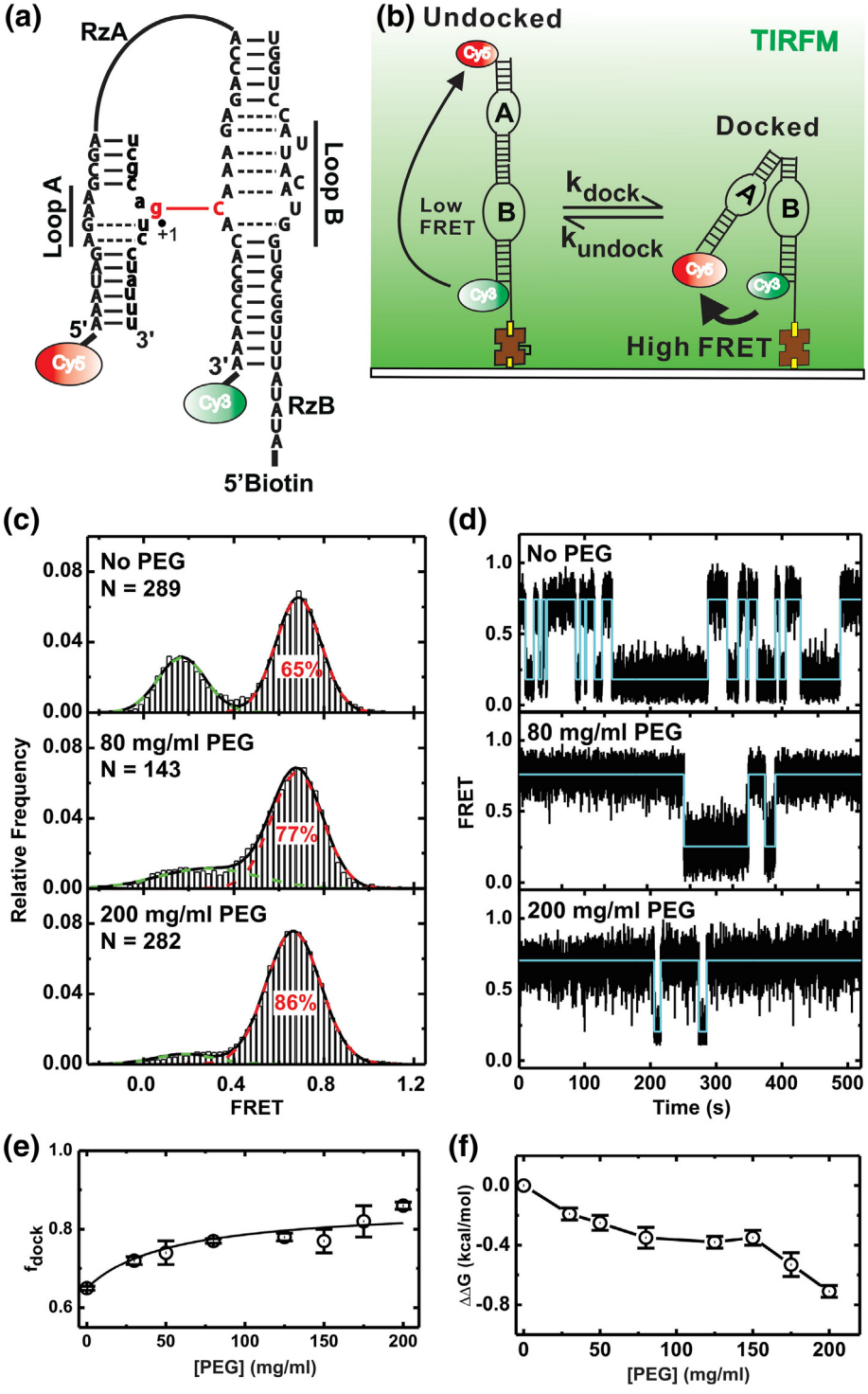

Fig. 1 (*legend on previous page*)

(Fig. 1c and Supplementary Fig. S1a) show that, as the PEG concentration is increased, there is a significant shift of the molecule population toward the high-FRET state. Plotting the transition occupancy density plots [42] from idealized hidden Markov models for molecules at different PEG concentrations revealed a growth in the fraction of high-FRET molecules found on the diagonal, that is, appearing static within the observation window (Supplementary Fig. S1b), indicating that the increase in docked-state fraction upon the addition of PEG results partially from stabilization of an (almost) static docked state. Accordingly, the rate of switching between the two FRET states develops in non-monotic fashion as increasingly fewer molecules still show such transitions (Fig. S2). Plotting the fraction of docked population as a function of increasing PEG concentration revealed an increase that saturates at 86% with a half-saturation point of PEG_{50} = 54 ± 10 mg/mL (Fig. 1e). Consistent with previous studies of this and other nucleic acids [1,4,6,10,14,15], we thus found the linear, high-molecular-weight polymer PEG8000 to stabilize RNA tertiary structure, in this case the docked state of the hairpin ribozyme.

Next, we converted the FRET histograms into values for the docking Gibbs free energy, ΔG_{dock}, as follows:

$$K_{dock} = \frac{\text{fraction docked}}{\text{fraction undocked}}; \Delta G_{dock} = -RT \ln(K_{dock})$$

Calculation of $\Delta\Delta G_{dock}$ relative to the absence of PEG revealed an additional stabilization of the docked state by approximately −0.7 kcal/mol at 200 mg/mL (or 20% w/v) PEG (Fig. 1f), within error similar to a recent report [10], We observed a marked 24% increase in the docked fraction upon the addition of PEG to 200 mg/mL (or 20% wt/vol) in 12 mM Mg^{2+} (Fig. 1e), corresponding to stabilization of the docked state by $\Delta\Delta G_{dock}$ ~ −0.8 kcal/mol.

Studies of different RNAs, including the hairpin ribozyme, have shown the prerequisite of a high divalent ion concentration for stabilizing the folded RNA [6,14,15,34,43]. We therefore performed smFRET studies at a constant PEG8000 concentration (200 mg/mL) in standard reaction buffer while varying the Mg^{2+} concentrations (1, 5, and 12 mM). The resulting FRET histograms (Fig. 2) show that at near-physiological Mg^{2+} concentration (1 mM) and

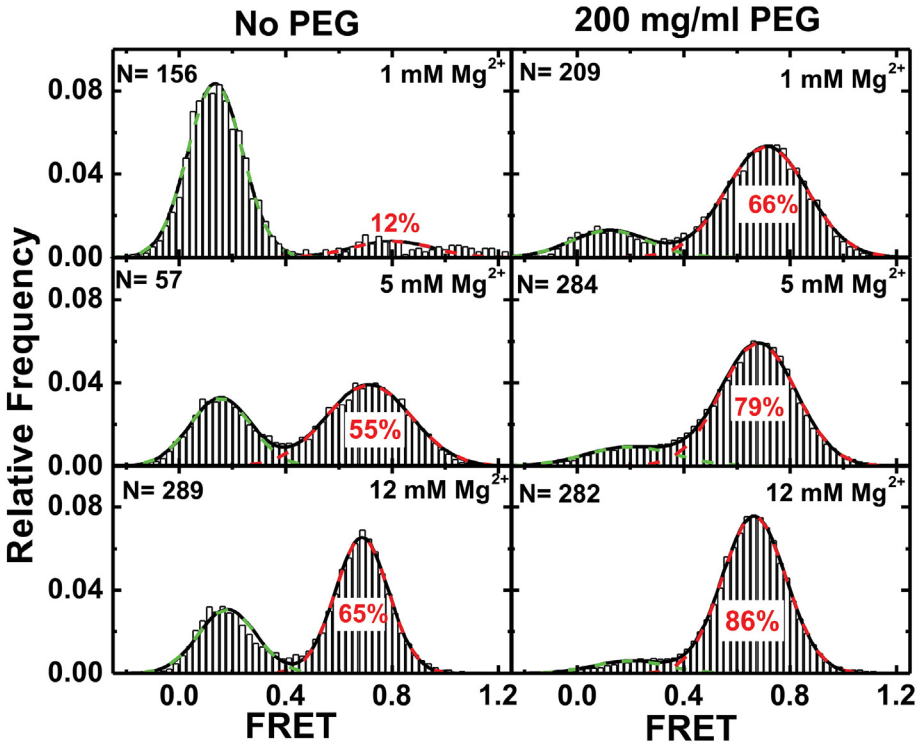

Fig. 2. The presence of PEG lowers the requirement of Mg^{2+} in stabilizing the active docked conformation of the hairpin ribozyme. FRET histograms built from N single-molecule time trajectories at different magnesium concentrations (1, 5 and 12 mM) in the absence of PEG (left) or presence of 200 mg/mL PEG (right). The FRET distributions reveal an increase of the high-FRET state population (docked conformation) as the Mg^{2+} concentration is increased. Comparing the left and right panels reveals that PEG effectively lowers the requirement for Mg^{2+} in stabilizing the docked conformation.

without PEG, only a small docked fraction (~12%) was observed. Upon adding PEG to this solution, a dramatic increase in the docked population to ~66% occurred. In the absence of PEG, increasing the Mg^{2+} concentration from 1 to 12 mM similarly increases the fraction docked from 12% to 65%, while in the presence of 200 mg/mL PEG, a more modest increase from 66% to 86% was observed. We thus found that the addition of 200 mg/mL PEG has a stabilizing effect similar to raising the Mg^{2+} concentration from 1 to 12 mM. That is, PEG approaching the intracellular concentration of macromolecular crowders (20%–40% of total volume [1,3,4,20]) facilitates the formation of a compact docked RNA conformation at near-physiological concentrations of free Mg^{2+} (0.5–2 mM [44]). Cleavage experiments suggest that PEG in parallel activates the ribozyme more at a lower than a higher Mg^{2+} concentration (Supplementary Fig. S3), indicating that the PEG-stabilized conformation is catalytically active, as expected from prior ribozyme studies [10,43].

Our results thus suggest that macromolecular crowding stabilizes the compact, natively folded conformation of the hairpin ribozyme under near-physiological concentrations of Mg^{2+}, as previously suggested for this and other RNAs [6,10,14,15]. This observation is consistent with previous work in which PEG lowered the Mg^{2+} threshold to forming natively folded RNA and DNA structures, generally thought to be mediated by volume excluded by the model crowder [1,6,10,14,45,46].

To investigate potential volume exclusion effects of PEG on hairpin ribozyme folding, we used a hard-sphere model that has been previously applied to smFRET experiments on a model RNA system [6]. In that study, Dupuis *et al.* [6] observed an increase in the population of the docked state of their tetraloop–tetraloop receptor system upon the addition of PEG that was primarily due to entropic effects. This finding suggested that PEG likely does not interact with either the docked or undocked conformation, but rather favors docking largely through EV effects. Accordingly, the authors found that their observations could be modeled very well using "scaled particle theory," which assumes that the crowder forms an ideal solution, and that the crowder and RNA exhibit only hard-sphere interactions [47,48]. This theory yields an analytical expression for the free energy change $\Delta G^{\mathrm{dil}\,\rightarrow\,\mathrm{crd}}$ upon the addition of a spherical co-solute of radius r_c at a volume fraction φ to a spherical particle of radius r_i:

$$\Delta G_i^{\mathrm{dil}\rightarrow\mathrm{crd}}/RT = -\ln(1-\varphi) + \left(\frac{\varphi}{1-\varphi}\right)\left(z^3+3z^2+z\right) + \left(\frac{\varphi}{1-\varphi}\right)^2\left(3z^3+\frac{9}{2}z^2\right) + \left(\frac{\varphi}{1-\varphi}\right)^3\left(3z^3\right)$$

where $z = r_i/r_c$ is the ratio of RNA to PEG radii. Through a thermodynamic cycle, this change in free energy upon insertion of the folded or unfolded RNA into a crowded solution maps directly onto our experimental observable, the free energy change upon RNA folding under crowded and dilute conditions.

The theory predicts a continuous decrease of $\Delta\Delta G$ with increasing PEG concentration, as found for the tetraloop–tetraloop receptor system. In contrast, for the hairpin ribozyme, we observed an initial decrease of $\Delta\Delta G$ that, in the presence of 1 mM Mg^{2+}, saturates above $\varphi \sim 0.08$ (Fig. 3a). In the presence of 12 mM Mg^{2+}, the saturation occurs at an even lower φ (~0.03) (Fig. 3b); a significant further drop in $\Delta\Delta G$ at $\varphi = 0.21$ hints at the possibility of a second regime, perhaps one in which EV effects begin to play a more significant role again. The combined data under 1 and 12 mM Mg^{2+} reveal a departure from the hard-sphere model over a ΔG_{dock} range of 0.9 to −1.5 kcal/mol.

The rapid drop in $\Delta\Delta G$ we observed at low PEG concentrations could implicate a soft, repulsive interaction between crowder and solute to yield a larger than expected effective EV [49]. However, the saturation we observed at higher PEG concentrations is more consistent with a "native state binding" (NSB) model in which the crowder exhibits weakly stabilizing (and thus likely non-specific) interactions with the folded solute [50]. We therefore investigated an NSB model, assuming that PEG has affinities for the docked and undocked conformations represented by dissociation constants $K_{\mathrm{D,dock}}$ and $K_{\mathrm{D,undock}}$, respectively. At a given [PEG], this affinity adds a term to $\Delta G^{\mathrm{dil}\,\rightarrow\,\mathrm{crd}}$ equal to the ΔG for binding of PEG to the ribozyme, multiplied by the fraction of ribozymes that are bound by PEG:

$$\Delta G_i^{\mathrm{dil-crd}}/RT = \ln[K_{\mathrm{D}}]\frac{[\mathrm{PEG}]}{[\mathrm{PEG}]+K_{\mathrm{D}}}$$

Like the component of $\Delta G^{\mathrm{dil}\,\rightarrow\,\mathrm{crd}}$ resulting from EV, a thermodynamic cycle maps this free energy change upon binding of PEG to the docked and undocked conformations of the ribozyme onto our experimental observable. Combining this NSB contribution to $\Delta\Delta G$ with the scaled particle theory-predicted EV contribution yielded a three-variable (r_{undock}, $K_{\mathrm{D,dock}}$ and $K_{\mathrm{D,undock}}$) hybrid model. Fits of this model to our data are plotted in Fig. 3, and the results of all EV, NSB and hybrid fits are quantified in Supplementary Table 1. Our 1-mM Mg^{2+} results are described entirely by the NSB component of the model, although it is likely that at higher PEG concentrations, EV effects become more important. Our 12-mM Mg^{2+} results are best described by the hybrid model.

The departure of our system from hard-sphere behavior makes it a potential model to further test different "soft interaction" theories of macromolecular crowding [51]. Taken together, our data suggest that PEG as a molecular crowder stabilizes the

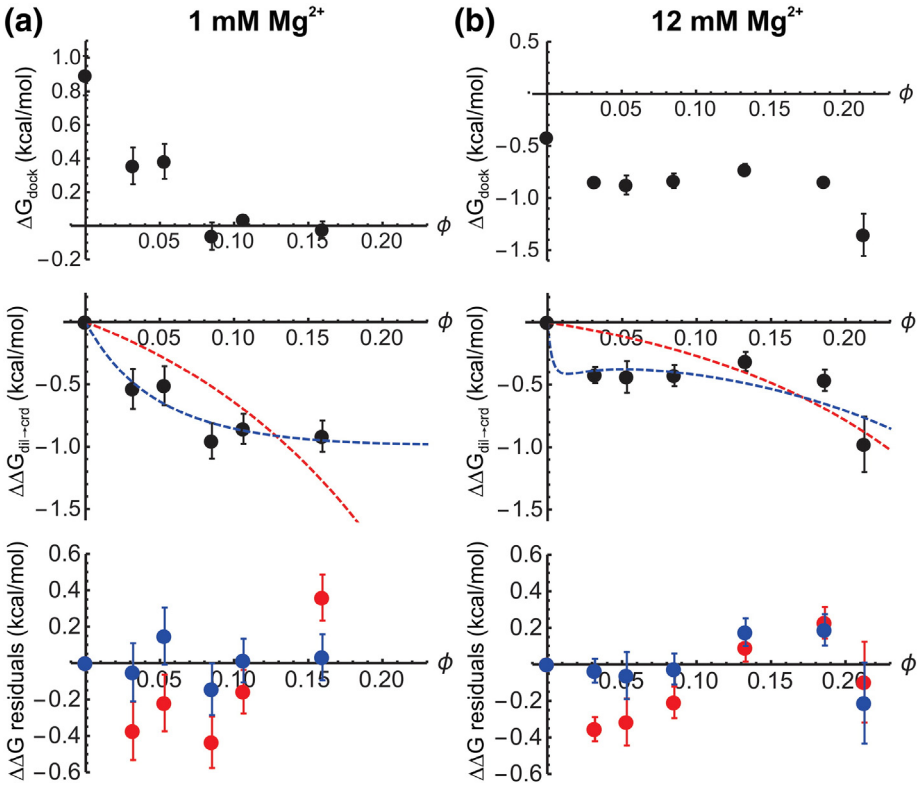

Fig. 3. Soft interactions, rather than EV, drive ribozyme folding. (a) ΔG_{dock} (top), $\Delta\Delta G_{dil \rightarrow crd}$ (middle) and fit residuals (bottom) as a function of PEG volume fraction φ at 1 mM Mg^{2+}. A fit of the scaled particle theory EV model to $\Delta\Delta G_{dil \rightarrow crd}$ is shown as a dashed red line, and a fit of the hybrid EV/NSB model is shown as a dashed blue line. Residuals for the EV model are plotted in red, and residuals for the hybrid model are plotted in blue. (b) ΔG_{dock} (top), $\Delta\Delta G$ with EV and hybrid fits (middle) and residuals at 12 mM Mg^{2+}. The fitting parameters obtained with each model are given in Supplementary Table 1.

folded conformation of the hairpin ribozyme, especially at physiological Mg^{2+} concentrations, through effects involving soft interactions between PEG and the RNA that can be either repulsive or attractive, rather than acting only through hard-sphere EV effects that are typically assumed to dominate [6,10,14,15,45].

Hairpin ribozyme folding in yeast extract is dominated by interactions with specific proteins

Having observed that the hairpin ribozyme exhibits unexpected soft interactions with PEG, a relatively inert and homogeneous model crowding agent, we next sought to examine the interaction of the ribozyme with cellular crowders, which encompass a wide variety of sizes, structures and chemical functionalities. To examine the folding of the hairpin ribozyme under cell-like conditions, we performed smFRET experiments in an established intracellular-mimic buffer [52] [30 mM Pipes (pH 7.5), 10 mM NaCl, 130 mM K^+ gluconate, 10 mM dithiothreitol (DTT), 1 mM ATP, 2.5 mM $Mg(OAc)_2$] in the presence of varying concentrations of yeast WCE. The resulting FRET histograms (Fig. 4a) again showed the undocked and docked conformations of the hairpin ribozyme as low- and high-FRET states, respectively (Fig. 4b). In buffer alone, only ~14% of the molecular population resides in the high-FRET state, increasing significantly to ~32% in the presence of just 0.1 mg/mL extract (measured as protein content; Fig. 4a, c and Supplementary Fig. S4a), a concentration 3 orders of magnitude lower than cellular protein concentrations. Increasing the yeast extract concentration further raises the population in the docked state to 43% in 0.9 mg/mL WCE and 70% in 14 mg/mL WCE. Cleavage assays in WCE were inconclusive due to non-specific substrate degradation (not sufficiently blocked by RNase inhibitor). Nevertheless, the similar average E_{FRET} of the high- and low-FRET states in WCE, PEG and dilute solution, which are unequivocally attributable to the intact full-length ribozyme–substrate complex, suggests that similar conformations, including the catalytically active docked conformation, are being sampled. Both FRET states are quite broad and dynamic (Fig. 4a, b), and a subset of traces shows rapid fluctuations within the low-FRET envelope (Supplementary Fig. S4), consistent with the notion that the ribozyme experiences a variety of different transient interactions with

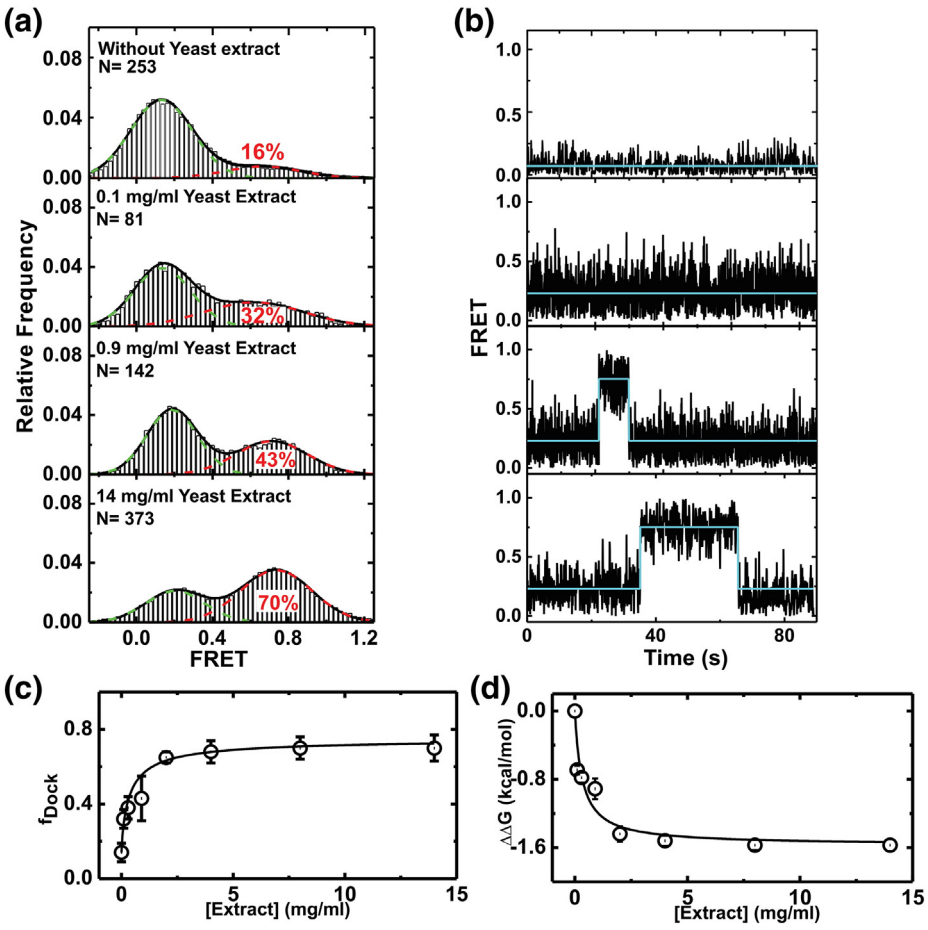

Fig. 4. Effect of WCE on docking of the hairpin ribozyme. (a) FRET histograms in the presence of 0, 0.1, 0.9 and 14 mg/mL yeast WCE, as indicated. The undocked low-FRET and docked high-FRET states were observed and fitted with Gaussian distributions (green and red fits, respectively). (b) Representative trajectories of dynamic molecules observed at, from top to bottom, 0.1, 0.9 and 14 mg/mL WCE, respectively. The FRET values fluctuated between the undocked low-FRET state and the docked high-FRET state. (c) Fraction of docked molecules fitted with a non-cooperative binding isotherm (black line) as a function of WCE concentration. (d) The change in the docking Gibbs free energy $\Delta\Delta G_{dock}$ as a function of WCE concentration revealed stabilization of the docked state by −1.6 kcal/mol in the presence of saturating concentrations of yeast WCE.

components of the extract. Notably, the fraction of docked population as a function of WCE concentration fits well with a non-cooperative binding isotherm with a half-saturation point of $K_{1/2}$ = 2 mg/mL WCE (Fig. 4c), consistent with a model that includes at least transient interactions of the hairpin ribozyme with RNA-binding proteins within the WCE. We used the relative areas of the docked high-FRET peak in the histograms of Fig. 4a and Supplementary Fig. S4b to calculate the docking Gibbs free energy $\Delta\Delta G_{dock}$ relative to the absence of WCE, which shows stabilization of the docked state by −1.6 kcal/mol at saturating concentrations of WCE. Dramatically (~10- to 40-fold) higher concentrations of PEG are required to achieve comparable stabilization (compare Figs. 1 and 2 with Fig. 4).

Our observation that yeast WCE favors docking at drastically lower concentrations than PEG suggests that the extract components not only act as molecular crowders but also provide chaperone-like activity by binding to and compacting the hairpin ribozyme. To identify proteins in the extract that interact with the hairpin ribozyme, we performed a native electrophoretic mobility shift assay (EMSA) under near-physiological conditions (Fig. 5). The free RNA (enzyme alone or in complex with a non-cleavable substrate analog) migrates as a single band with significant Cy3 and Cy5 fluorescence intensities, indicating an, on average, intermediate FRET value. When interacting with molecules in the extract, the corresponding bands are expected to migrate more slowly; at least three such bands were observed

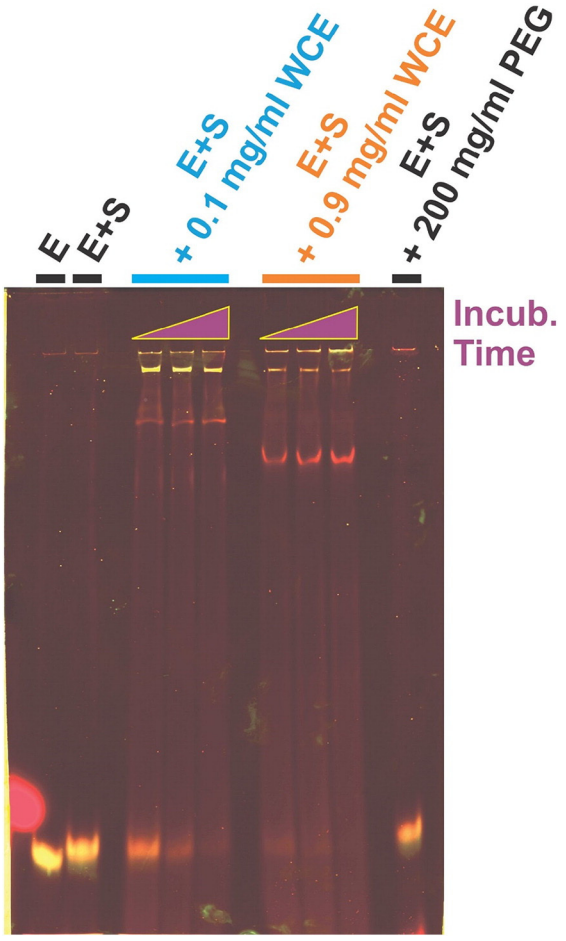

Fig. 5. Binding of proteins in yeast WCE to the hairpin ribozyme. An 8% non-denaturing gel EMSA was run under near-physiological conditions. The free RNA (enzyme alone (E) and the enzyme:non-cleavable substrate analog complex (ES)) migrate as single bands. After incubating in yeast WCE (0.1 or 0.9 mg/mL extract) for different durations (left to right: 5, 30 and 90 min), slower-migrating bands are observed. A negative control was run in the presence of 200 mg/mL PEG. The image was generated by overlaying scans of Cy3 and Cy5 emission (in green and red, respectively) obtained upon excitation of Cy3.

depending on the concentration of WCE and incubation time prior to the EMSA. In some of these bands, the Cy5 signal is clearly enhanced, indicating that binding induces higher FRET values and therefore more docking (Fig. 5).

To identify the proteins in these shifted bands, the main bands were excised and an affinity pull-down assay was performed wherein the excised bands were eluted, the biotinylated hairpin ribozyme bound to streptavidin-coated Dynabeads, and all co-bound proteins eluted using SDS. A control with the RNA omitted was performed in parallel, and both samples were analyzed by mass spectrometry. The spectrum counts obtained under both conditions were normalized to the number of the total spectrum counts to determine the fraction of each detected protein. With this normalized scale, a protein fraction is countable when the value is more than 0.01 ($\geq$10 spectrum counts). The difference scale between sample and control reveals proteins enriched in the presence of hairpin ribozyme, including HSC 82 protein, Hsp 71, and several key enzymes of the glycolytic pathway, including pyruvate kinase (PK) and phosphoglycerate kinase (PGK) (Fig. 6a and Supplementary Table 2). An EMSA with readily available purified proteins similarly revealed RNA-binding capabilities of particularly the purified PGK and glucose 6-phosphate dehydrogenase (G6PDH) enzymes (Fig. 6b). As negative controls, we also tested several proteins that were not found to bind the ribozyme, and unrelated proteins from other organisms. Specifically, bovine serum albumin and glyceraldehyde 3-phosphate dehydrogenase did not bind to the ribozyme in our EMSAs (Fig. 6b). Furthermore, these proteins, in addition to casein, did not impact the FRET histogram of the ribozyme even at much higher concentrations than needed for yeast extract (Fig. S5). While to date there have been no studies identifying cellular proteins that bind to the hairpin ribozyme, previous reports revealed non-glycolytic functions of PK and PGK. These include binding to transcription factors such as Oct447 and binding to single-stranded RNA, ribosomal RNA, telomerase RNA, untranslated regions of several mRNAs and RNA chaperones to viruses such as hepatitis C virus [53–56]. By showing that binding results in stabilization of the native conformation of the ribozyme, our data significantly expand the functional significance of these proteins as potential cellular RNA folding chaperones.

Most studies of macromolecular crowding have utilized high concentrations of model crowder, in the range of tens to hundreds of milligrams per milliliter; however, similar to our observations, some recent studies have revealed that for certain systems, “crowding” effects are observable at much lower co-solute concentrations. For example, it has been found that the picosecond-timescale solvation dynamics of serum albumins are perturbed at co-solute concentrations as low as 2 mg/mL of PEG8000 and Dextran 6 [57]. The apparent saturation of hairpin ribozyme folding around 30–80 mg/mL PEG (Fig. 1e) and 1–5 mg/mL of yeast WCE proteins (Fig. 4c) suggests a departure from an EV model, which we confirmed by the poor fit of scaled particle theory to our PEG data (Fig. 3). Rather, the saturation effects observed in our PEG and, in particular, WCE titrations are better fit by a non-cooperative binding isotherm, indicating stabilization of the docked conformation via direct binding of the “crowder” to the RNA (captured in our modeling by the NSB contribution). Such direct interactions between PEG and hydrophobic residues in some proteins have been reported, although these

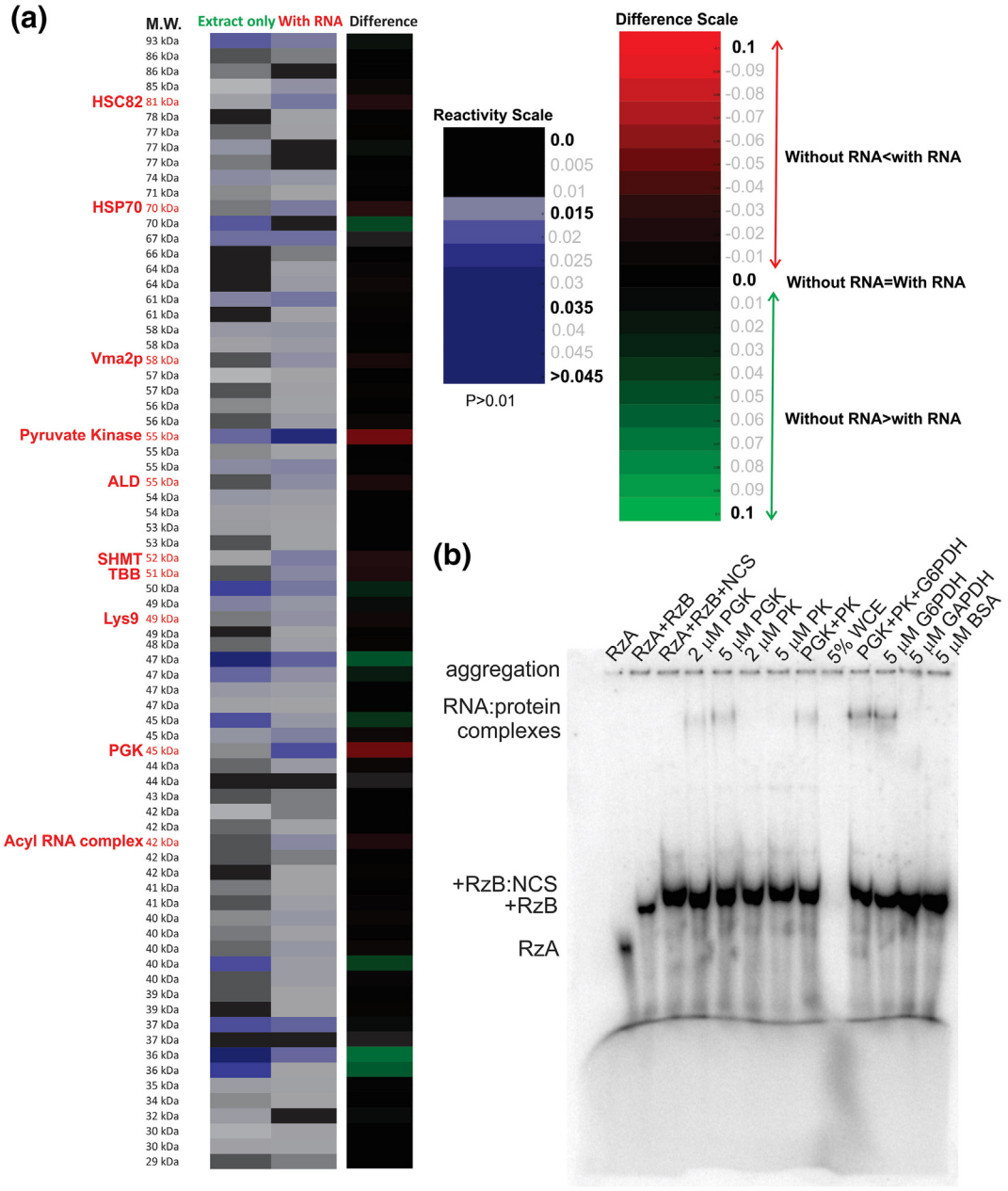

Fig. 6. Identification through mass spectrometry and EMSA of specific proteins from yeast WCE binding the hairpin ribozyme. (a) The peptides obtained after isolation and digestion of the hairpin ribozyme–protein complexes were analyzed using nano LC–MS/MS. This analysis was done in parallel with a sample without hairpin ribozyme. The spectral counts obtained under each condition were normalized to the number of total spectral counts to determine the fraction of each detected protein. The difference map between the samples with and without ribozyme yields information about protein enrichment when the hairpin ribozyme is present (highlighted in red). These results are summarized in Supplementary Table 2. (b) Native 8% polyacrylamide EMSA showing binding of PGK and G6PDH to the hairpin ribozyme in the form of slowly migrating RNA:protein complexes.

interactions typically destabilize the native fold of the protein by favoring solvent accessibility of these residues [20,58]. We observe that an RNA structure instead is stabilized by binding of PEG, suggesting that future mechanistic work is needed to understand these interactions. In the case of WCE, our direct binding hypothesis was powerfully supported by EMSA and affinity pull-down assays, identifying several ubiquitously expressed metabolic enzymes such as PK, PGK and G6PDH as RNA-binding proteins (Figs. 5 and 6).

RNA–protein complexes are involved in many central biological processes [59,60]. In addition to their main cellular function, RNA-binding proteins have frequently been found to "moonlight," including acting as folding chaperones to help RNA attain a specific structure or function [61]. Our results are consistent with an emerging picture in which numerous, especially metabolic, proteins conserved from yeast to man harbor non-canonical RNA binding domains [40,41,56,62,63]. Moving beyond the pure observation of their existence, we here have assigned these pervasive RNA:protein interactions a specific function in folding an RNA into its native docked structure, complementing a reciprocal chaperoning role recently emerging for negatively charged RNAs [64], polyphosphates [65] and even ATP [66] in stabilizing soluble proteins. The high diversity of protein sizes, shapes, functional moieties and thus surface charges appears to enable unexpected, transient (weak), yet numerous and thus in sum powerful interactions with RNA that enhance the physiological functions of both biopolymers within the low-counterion environment of the cell.

Conclusions

In summary, we have demonstrated that macromolecular crowding by both PEG and yeast WCE stabilizes the native, docked state of the hairpin ribozyme. We have demonstrated that at moderate concentrations of PEG, this results from soft interactions that potentially include long-range repulsion and/or direct binding of PEG to the docked conformation of the ribozyme. In the case of WCE, we show that this stabilization likely involves specific binding of proteins to the ribozyme, including the ones that are not canonical RNA-binding proteins. Our results demonstrate that "crowding" in the cellular environment is the result of many different types of interactions that together serve to fine-tune the structures and functions of RNA molecules.

Materials and Methods

RNA purification and labeling

Three RNA strands (fluorophore-labeled RzA, biotinylated RzB and non-cleavable substrate analogue NCS) were used to assemble the two-way junction hairpin ribozyme (Fig. 1a). RNAs were purchased from the Keck Foundation Resource Laboratory at the Yale University School of Medicine. The 2′-hydroxyl protection groups were removed following the manufacturer's protocol[†]. The RNA was purified by denaturing gel electrophoresis (20% w/v polyacrylamide, 8 M urea). RNAs were gel eluted using the Crush-n-soak method against elution buffer [0.5 M NaOAc (pH 5.3), 0.1 mM EDTA) overnight at 4 °C, followed by chloroform extraction, ethanol precipitation and C18 reverse-phase HPLC. The 3′-end C7 amino linker on RzA was labeled with succinimidyl-ester Cy3 (GE Healthcare) in labeling buffer (0.1 M sodium carbonate, pH 8.5) overnight at room temperature. This step was followed by ethanol precipitation and C18 reverse-phase HPLC. RNA concentrations were measured using a NanoDrop spectrometer and calculated after background subtraction [67].

smFRET

Single-molecule experiments were performed as described [32,34]. The two ribozyme strands (RzA and RzB, at 1 μM and 500 nM, respectively) were heated at 90 °C in standard buffer [50 mM Tris–HCl (pH 7.5), 12 mM $MgCl_2$, unless other specified] for 45 s before cooling to room temperature over 15 min. We diluted the annealed strands to 50–100 pM and immobilized the hybrid onto a PEGylated slide through a biotin–streptavidin linkage. Non-cleavable substrate analog (200 nM) with 2′-*O*-methyl modification (NCS) at the cleavage site was added with the oxygen scavenger system to suppress catalysis without altering the docking behavior [68]. The oxygen scavenger system composed of 50 nM protocatechuate dioxygenase, 5 mM protocatechuate and 2 mM Trolox was used to minimize photobleaching and blinking of the fluorophores [69]. Imaging by TIRFM at room temperature (17–20 °C) in a microfluidic channel was performed in either standard ribozyme reaction buffer [32,34] [50 mM Tris–HCl (pH 7.5), 12 mM $MgCl_2$] or an intracellular-mimic buffer established by Edmonds *et al*. [52], consisting of 30 mM Pipes (pH 7.5), 10 mM NaCl, 130 mM K^+ gluconate, 10 mM DTT, 1 mM ATP and 2.5 mM $Mg(OAc)_2$ concentration. Intracellular-mimic buffer was made fresh and filtered with a 0.2 μm Ultra-free-MC filter (Millipore) before each experiment.

We excited the donor fluorophore (Cy3) in a home-built TIRFM setup with a green laser (532 nm, ~12 mW). We separated emission from the donor and acceptor using a dichroic mirror (Chroma 610DCXR), filtered them individually (Chroma HQ580-60 M and HQ655LP) and detected them as side-by-side images on an intensified CCD camera (I-Pentamax, Princeton Instruments). FRET histograms were constructed and dwell times determined for each docking and undocking event as described [42]. Cumulative dwell time histograms were fitted with single- or double-exponentials, similar to those described for the cleavage assays, to determine k_{dock} and k_{undock} as described [32,33]. FRET histograms were fitted with Gaussian functions to determine the relative molecular fractions in the low- and high-FRET peaks as the relative areas, whereas the dependencies of the docked fraction on the

PEG and WCE concentrations were fitted with non-cooperative binding isotherms.

Cleavage assays

Cleavage reactions were performed under single-turnover conditions in a standard reaction buffer at room temperature as previously described [32,33]. Briefly, the ribozyme strands (RzA and RzB) were heated at 90 °C for 45 s in the absence of $MgCl_2$, followed by slow cooling over 15 min at room temperature after adding $MgCl_2$. PEG was added at 200 mg/mL and allowed 5 min to equilibrate. Less than 4 nM 5′-end radioactively labeled substrate was mixed with the ribozyme upon diluting the enzyme to 200 nM. Aliquots of the reaction were removed at varying time points and quenched with an equal volume of loading buffer (60 mM EDTA, 95% formamide). The 5′-cleavage product was separated from uncleaved substrate by a denaturing, 8 M urea, 20% (w/v) polyacrylamide gel electrophoresis, and was quantified and normalized to the sum of the substrate and product bands by using a Typhoon 9410 Variable Mode Imager (GE Healthcare Life Sciences) with ImageQuant software (Molecular Dynamics). The fraction cleaved was fitted with a double-exponential function of the form:

$$y(t) = y_0 + A_1\left(1-e^{-k_{\text{fast}}*t}\right) + A_2\left(1-e^{-k_{\text{slow}}*t}\right),$$

where (A_1 + A_2) is the final extent of the cleavage and k_{fast} (k_f) and k_{slow} (k_s) are the apparent rate constants, respectively [32,33]. Error bars were calculated from typically three independent assays.

Modeling of PEG titrations

Application of scaled particle theory to macromolecular crowding has been explained in detail elsewhere [6]. Briefly, this approach assumes the presence of ideal solutions of co-solute particles, and hard-sphere interactions between particle pairs with effective radii of gyration for each of the co-solutes. As described in the Results and Discussion section, this theory yields an analytical expression for the free energy change $\Delta G_i^{\text{dil}\rightarrow\text{crd}}$ upon the addition of a spherical co-solute of radius r_c at a volume fraction φ to a spherical particle of radius r_i. φ was calculated as $\varphi = \frac{4\pi r_c^3}{3}\rho_c$, where ρ_c is the number density of the crowder (calculated using the mass density of the appropriate PEG solution [70]), and r_c is the radius of gyration of the crowder [71]. The effect of addition of the crowder on ribozyme docking is then given by:

$$\begin{aligned}\Delta\Delta G &= \Delta G_{\text{docked}}^{\text{dil}\rightarrow\text{crd}} - \Delta G_{\text{undocked}}^{\text{dil}\rightarrow\text{crd}} \\ &= \Delta G_{\text{dilute}}^{\text{undock}\rightarrow\text{dock}} - \Delta G_{\text{crowded}}^{\text{undock}\rightarrow\text{dock}}\end{aligned}$$

where $\Delta G_{\text{docked}}^{\text{dil}\rightarrow\text{crd}}$ and $\Delta G_{\text{undocked}}^{\text{dil}\rightarrow\text{crd}}$ differ only in the value of r_i. $r_{\text{dock}} = 26.27$ Å was measured from a crystal structure of the docked ribozyme [72]. Experimental $\Delta\Delta G$ values were calculated by fitting each FRET histogram with two Gaussians, and error bars were generated by bootstrapping. A least-squares fit was then performed with r_{undock} as the one free parameter. In the NSB contribution model, the free parameters were $K_{\text{D,dock}}$ and $K_{\text{D,dock}}$, the dissociation constants of complexes between PEG and the docked and undocked ribozyme, respectively. In the hybrid model, the contributions to ΔΔG from EV and NSB were added together, and a fit performed with all three free parameters. All fits were subject to the constraint that the radius of the undocked ribozyme r_{undock} be larger than the radius r_{dock} of the docked ribozyme.

WCE preparation

Yeast WCE was prepared in-house using the following protocol. One liter of yeast was grown in yeast extract peptone dextrose media until an OD600 of 1.6 to 2.0 was reached (after ~2 days). Yeast cells were harvested by centrifuging at 4500 rpm for 15 min. Pellets from the 1 L culture were suspended in 35 mL of AGK buffer [10 mM Hepes–KOH (pH 7.9), 1.5 mM $MgCl_2$, 200 mM KCl, 10% v/v glycerol, 0.5 mM DTT), then centrifuged again at 4500 rpm for 15 min at 4 °C. The pellets were combined and suspended in 30 mL of AGK buffer, 600 μM PMSF and 1.5 mM benzamidine, then centrifuged in a swinging bucket rotor at 2500 rpm for 10 min. The supernatant was completely decanted, and 0.4 volumes (based on the volume of the pellet) of AGK buffer with 600 μM PMSF and 1.5 mM benzamidine was added and vortexed to make a thick cell suspension. The suspension was frozen down as pellets by dropwise addition of the cell suspension to a 50-mL tube filled with liquid nitrogen. The frozen pellets were further mixed with liquid nitrogen and then ground up using a mortar and pestle pre-cooled in liquid nitrogen until a fine powder was formed. The powder was thawed at 4 °C in a water-ice bath for 30 to 40 min. The cell lysate was centrifuged at 17,000 rpm for 30 min at 4 °C using a SS-34 fixed angle rotor (Thermo Scientific). The supernatant was transferred to another pre-chilled ultracentrifuge tube and spun at 37,000 rpm for 80 min at 4 °C in a type 70 Ti rotor (Beckman Coulter). The second layer from the top was removed and dialyzed twice (MWCO 14,000–16,000 Da) against 2 L of dialysis buffer [20 mM Hepes–KOH (pH 7.9), 0.2 mM EDTA, 50 mM KCl, 20% v/v glycerol, 0.5 mM DTT] at 4 °C for 1.5 h at a time. After dialysis, cell extract was microcentrifuged at 13,000 rpm for 5 min at 4 °C, then frozen in liquid nitrogen in 50 μL aliquots and stored at −80 °C until further use. The protein concentration of this yeast WCE was determined by Bradford assay (Bio-Rad kit) and was normally 12 to 20 mg/mL.

EMSAs

Native (non-denaturing) electrophoretic gel shift assays were performed as previously described [73], using 8% non-denaturing polyacrylamide gel electrophoresis between low-fluorescence glass plates with a running buffer consisting of 50 mM Tris–acetic acid (pH 7.5) and 2.5 mM $Mg(OAc)_2$. Solutions of doubly-fluorophore-labeled hairpin ribozyme (10 pmol) were annealed by heating at 90 °C in intracellular-mimic buffer for 45 s and slow cooling to room temperature. Different concentrations of yeast WCE were added followed by time course incubation (5, 30 and 90 min) at room temperature. An equal volume of 40% glycerol was added to each sample right before loading the gel. The gel was run for 6–7 h at 13 W maximum power and 4 °C, then scanned with a Typhoon 9410 Variable Mode Imager to detect Cy3 (excitation at 532 nm, 600 V PMT, 580 ± 30 nm band-pass emission filter), Cy5 (excitation at 633 nm, 600 V PMT and 670 ± 30 nm band-pass emission filter) and FRET (excitation at 532 nm, 600 V PMT, 670 ± 30 nm band-pass emission filter).

To study the binding of individual purified proteins to the hairpin ribozyme, 5′-radiolabeled RzA was heat annealed with RzB and NCS in a 1:5:100 ratio by heating to 90 °C for 2 min, then cooling to RT over 15 min. $MgCl_2$ was added to 12 mM immediately after heating. Mixtures lacking RzB and/or NCS were prepared analogously to confirm assembly of the ribozyme. The annealed mixture was diluted into a solution containing intracellular-mimic buffer, 20 units of rRNasin (Promega), and 2–5 μM of the protein of interest, and incubated at RT for 60 min. An equal volume of 40% glycerol was then added to each sample, and the samples were resolved on a native 8% polyacrylamide gel run in 0.25× TBE buffer at 4 °C. Bovine serum albumin and glyceraldehyde 3-phosphate dehydrogenase were included as negative controls.

Affinity pull-down assay

The shifted bands observed in the non-denaturing polyacrylamide gel after incubation with WCE were excised and placed into a Nanosep centrifugal device equipped with a membrane with MWCO (3 K). The elution buffer (0.25 M Tris–HCl, pH 6.8) was added directly to the centrifugal device, mixed with the gel pieces by vortexing, followed by centrifugation at 14,000*g* for 20 min. The filtrate eluents were concentrated using a new Nanosep centrifugal device equipped with a 3K-MWCO membrane. This step was followed by a Bradford assay to estimate the protein concentration in the eluate. To further purify only the proteins that bind the biotinylated hairpin ribozyme, magnetic Dynabeads MyOne streptavidin C1 were added following the manufacturer protocol to specifically capture all biotinylated RNA:protein complexes. After washing the beads with 10 mM Tris–HCl (pH 7.5), 0.1 mM EDTA and 1 M NaCl, proteins were released from the beads using TEN250 buffer [10 mM Tris–HCl (pH 7.5), 0.1 mM EDTA, 250 mM NaCl] in the presence of 2× SDS buffer [100 mM Tris–HCl (pH 6.8), 4% (w/v) SDS, 0.2% (w/v) bromophenol blue, 20% glycerol, 200 mM β-mercaptoethanol]. The eluted proteins were subjected to denaturing SDS-polyacrylamide gel electrophoresis. The resulting bands were analyzed by mass spectrometry.

Mass spectrometry

Gel bands were reduced with DTT, alkylated with iodoacetamide and digested at 37 °C overnight using trypsin. The resulting peptides were analyzed using nano LC–MS/MS on a ThermoScientific Orbitrap Velos mass spectrometer. Product ion data were searched against the NCBI protein database using the Mascot and X! Tandem search engines. The threshold was chosen based on spectral count scoring to distinguish correct peptide identifications. This identification is a probability based on the peptide sequences that are derived from peptide fragmentation spectra and matched against protein sequences available in the NCBI database. The minimum requirement for protein identification is two completely sequenced unique peptides per proteins. Mascot output files were parsed into the Scaffold program[‡] for filtering to assess false discovery rates and allow only correct protein identifications.

Acknowledgments

We thank M. Kahlscheuer for his help in preparing the WCE, H. Remmer for her assistance in the mass spectrometry data analysis and P. Lund for helpful discussions. This research was funded by National Institutes of Health R01 grant GM062357 to N.G.W., and J.R.W. acknowledges support from National Institutes of Health K99/R00 award GM120457.

Author Contributions: The manuscript was written through contributions of all authors.

Appendix A. Supplementary data

The Supporting Information is available on the JMB Publications Web site. It includes four figures, containing additional smFRET data and ribozyme cleavage assays (PDF). Supplementary data associated with this article can be found in the online version at https://doi.org/10.1016/j.jmb.2017.10.030.

Received 23 August 2017;
Received in revised form 22 October 2017;
Accepted 30 October 2017
Available online 8 November 2017

Keywords:
hairpin ribozyme;
single-molecule fluorescence resonance energy transfer;
molecular crowding;
transient RNA–protein interactions;
polyethylene glycol

Present address: M. Daher, Department of Chemistry and Biochemistry, University of Detroit Mercy, Detroit, MI 48221-3038, USA.

†http://medicine.yale.edu/keck/oligo/services/protocols/RNA.aspx
‡www.proteomesoftware.com

Abbreviations used:
PEG, polyethylene glycol; WCE, yeast whole cell extract; NCS, non-cleavable substrate analog with 2′-*O*-methyl modification; TIRFM, total internal reflection fluorescence microscopy; EV, excluded volume; NSB, native state binding; EMSA, electrophoretic mobility shift assay; PK, pyruvate kinase; PGK, phosphoglycerate kinase; G6PDH, glucose 6-phosphate dehydrogenase.

References

[1] S.-i. Nakano, H. Karimata, T. Ohmichi, J. Kawakami, N. Sugimoto, The effect of molecular crowding with nucleotide length and cosolute structure on DNA duplex stability, J. Am. Chem. Soc. 126 (2004) 14330–14,331.
[2] A.B. Fulton, How crowded is the cytoplasm? Cell 30 (1982) 345–347.
[3] S. Nakano, D. Miyoshi, N. Sugimoto, Effects of molecular crowding on the structures, interactions, and functions of nucleic acids, Chem. Rev. 114 (2014) 2733–2758.
[4] S.I. Nakano, N. Sugimoto, Model studies of the effects of intracellular crowding on nucleic acid interactions, Mol. BioSyst. 13 (2016) 32–41.
[5] M. Gao, D. Gnutt, A. Orban, B. Appel, F. Righetti, R. Winter, et al., RNA hairpin folding in the crowded cell, Angew. Chem. Int. Ed. 55 (2016) 3224–3228.
[6] N.F. Dupuis, E.D. Holmstrom, D.J. Nesbitt, Molecular-crowding effects on single-molecule RNA folding/unfolding thermodynamics and kinetics, Proc. Natl. Acad. Sci. U. S. A. 111 (2014) 8464–8469.
[7] J. Tyrrell, K.M. Weeks, G.J. Pielak, Challenge of mimicking the influences of the cellular environment on RNA structure by PEG-induced macromolecular crowding, Biochemistry 54 (2015) 6447–6453.
[8] Z.-J. Tan, S.-J. Chen, Ion-mediated RNA structural collapse: effect of spatial confinement, Biophys. J. 103 (2012) 827–836.
[9] A.V. Predeus, S. Gul, S.M. Gopal, M. Feig, Conformational sampling of peptides in the presence of protein crowders from AA/CG-multiscale simulations, J. Phys. Chem. B 116 (2012) 8610–8620.
[10] B.P. Paudel, D. Rueda, Molecular crowding accelerates ribozyme docking and catalysis, J. Am. Chem. Soc. 136 (2014) 16700–16,703.
[11] S.-i. Nakano, H.T. Karimata, Y. Kitagawa, N. Sugimoto, Facilitation of RNA enzyme activity in the molecular crowding media of cosolutes, J. Am. Chem. Soc. 131 (2009) 16881–16,888.
[12] S.-i. Nakano, Y. Kitagawa, H.T. Karimata, N. Sugimoto, Molecular crowding effect on metal ion binding properties of the hammerhead ribozyme, Nucleic Acids Symp. Ser. 52 (2008) 519–520.
[13] H. Karimata, S.-I. Nakano, N. Sugimoto, The roles of cosolutes on the hammerhead ribozyme activity, Nucleic Acids Symp. Ser. 50 (2006) 81–82.
[14] D. Kilburn, J.H. Roh, R. Behrouzi, R.M. Briber, S.A. Woodson, Crowders perturb the entropy of RNA energy landscapes to favour folding, J. Am. Chem. Soc. 135 (2013) 10055–10,063.
[15] D. Kilburn, J.H. Roh, L. Guo, R.M. Briber, S.A. Woodson, Molecular crowding stabilizes folded RNA structure by the excluded volume effect, J. Am. Chem. Soc. 132 (2010) 8690–8696.
[16] C.A. Strulson, J.A. Boyer, E.E. Whitman, P.C. Bevilacqua, Molecular crowders and cosolutes promote folding cooperativity of RNA under physiological ionic conditions, RNA 20 (2014) 331–347.
[17] K. Luby-Phelps, The physical chemistry of cytoplasm and its influence on cell function: an update, Mol. Biol. Cell 24 (2013) 2593–2596.
[18] S. Qin, H.-X. Zhou, A generalized fundamental measure theory for atomistic modeling of macromolecular crowding, Phys. Rev. E 81 (2010) 031919.
[19] D. Thirumalai, D.K. Klimov, G.H. Lorimer, Caging helps proteins fold, Proc. Natl. Acad. Sci. U. S. A. 100 (2003) 11195–11,197.
[20] H.X. Zhou, G. Rivas, A.P. Minton, Macromolecular crowding and confinement: biochemical, biophysical, and potential physiological consequences, Annu. Rev. Biophys. 37 (2008) 375–397.
[21] T. Ando, J. Skolnick, Crowding and hydrodynamic interactions likely dominate in vivo macromolecular motion, Proc. Natl. Acad. Sci. U. S. A. 107 (2010) 18457–18462.
[22] S.B. Zimmerman, A.P. Minton, Macromolecular crowding—biochemical, biophysical, and physiological consequences, Annu. Rev. Biophys. Biomol. Struct. 22 (1993) 27–65.
[23] Y. Chen, J.P. Potratz, P. Tijerina, M. Del Campo, A.M. Lambowitz, R. Russell, DEAD-box proteins can completely separate an RNA duplex using a single ATP, Proc. Natl. Acad. Sci. U. S. A. 105 (2008) 20203–20208.
[24] D. Herschlag, M. Khosla, Z. Tsuchihashi, R.L. Karpel, An RNA chaperone activity of non-specific RNA binding proteins in hammerhead ribozyme catalysis, EMBO J. 13 (1994) 2913–2924.
[25] R. Singh, J. Valcarcel, Building specificity with nonspecific RNA-binding proteins, Nat. Struct. Mol. Biol. 12 (2005) 645–653.
[26] M.J. Smola, J.M. Calabrese, K.M. Weeks, Detection of RNA–protein interactions in living cells with SHAPE, Biochemistry 54 (2015) 6867–6875.
[27] Z. Lu, H.Y. Chang, Decoding the RNA structurome, Curr. Opin. Struct. Biol. 36 (2016) 142–148.
[28] P.C. Bevilacqua, L.E. Ritchey, Z. Su, S.M. Assmann, Genome-wide analysis of RNA secondary structure, Annu. Rev. Genet. 50 (2016) 235–266.

[29] K.A. Leamy, S.M. Assmann, D.H. Mathews, P.C. Bevilacqua, Bridging the gap between in vitro and in vivo RNA folding, Q. Rev. Biophys. 49 (2016), e10.
[30] R.S. Yadava, E.M. Mahen, M.J. Fedor, Kinetic analysis of ribozyme–substrate complex formation in yeast, RNA 10 (2004) 863–879.
[31] N.G. Walter, J.M. Burke, The hairpin ribozyme: structure, assembly and catalysis, Curr. Opin. Chem. Biol. 2 (1998) 24–30.
[32] D. Rueda, G. Bokinsky, M.M. Rhodes, M.J. Rust, X. Zhuang, N.G. Walter, Single-molecule enzymology of RNA: essential functional groups impact catalysis from a distance, Proc. Natl. Acad. Sci. U. S. A. 101 (2004) 10066–10,071.
[33] X. Zhuang, H. Kim, M.J. Pereira, H.P. Babcock, N.G. Walter, S. Chu, Correlating structural dynamics and function in single ribozyme molecules, Science 296 (2002) 1473–1476.
[34] G. Bokinsky, D. Rueda, V.K. Misra, M.M. Rhodes, A. Gordus, H.P. Babcock, et al., Single-molecule transition-state analysis of RNA folding, Proc. Natl. Acad. Sci. U. S. A. 100 (2003) 9302–9307.
[35] S. Liu, G. Bokinsky, N.G. Walter, X. Zhuang, Dissecting the multistep reaction pathway of an RNA enzyme by single-molecule kinetic "fingerprinting", Proc. Natl. Acad. Sci. U. S. A. 104 (2007) 12634–12,639.
[36] I.M. Verma, N. Somia, Gene therapy—promises, problems and prospects, Nature 389 (1997) 239–242.
[37] S.J. Zeller, P. Kumar, RNA-based gene therapy for the treatment and prevention of HIV: from bench to bedside, Yale J. Biol. Med. 84 (2011) 301–309.
[38] T.O. Dorai, A. Carl, Aaron E. Katz, R. Buttyan, Development of a hammerhead ribozyme against bcl-2. I. Preliminary evaluation of a potential gene therapeutic agent for hormone-refractory human prostrate cancer, Prostate 32 (1997) 246–258.
[39] A.S.H. Lewin, W. William, Ribozyme gene therapy: applications for molecular medicine, Trends Mol. Med. 7 (2001) 221–228.
[40] B.M. Beckmann, R. Horos, B. Fischer, A. Castello, K. Eichelbaum, A.-M. Alleaume, et al., The RNA-binding proteomes from yeast to man harbour conserved enigmRBPs, Nat. Commun. 6 (2015) 10127.
[41] A. Castello, M.W. Hentze, T. Preiss, Metabolic enzymes enjoying new partnerships as RNA-binding proteins, Trends Endocrinol. Metab. 26 (2015) 746–757.
[42] M. Blanco, N.G. Walter, Analysis of complex single-molecule FRET time trajectories, Methods Enzymol. 472 (2010) 153–178.
[43] H.T. Lee, D. Kilburn, R. Behrouzi, R.M. Briber, S.A. Woodson, Molecular crowding overcomes the destabilizing effects of mutations in a bacterial ribozyme, Nucleic Acids Res. 43 (2015) 1170–1176.
[44] A.M. Romani, Cellular magnesium homeostasis, Arch. Biochem. Biophys. 512 (2011) 1–23.
[45] R. Desai, D. Kilburn, H.T. Lee, S.A. Woodson, Increased ribozyme activity in crowded solutions, J. Biol. Chem. 289 (2014) 2972–2977.
[46] J. Shin, A.G. Cherstvy, R. Metzler, Kinetics of polymer looping with macromolecular crowding: effects of volume fraction and crowder size, Soft Matter 11 (2015) 472–488.
[47] H. Reiss, H.L. Frisch, J.L. Lebowitz, Statistical mechanics of rigid spheres, J. Chem. Phys. 31 (1959) 369–380.
[48] J.L. Lebowitz, E. Helfand, E. Praestgaard, Scaled particle theory of fluid mixtures, J. Chem. Phys. 43 (1965) 774–779.
[49] M. Sarkar, C. Li, G.J. Pielak, Soft interactions and crowding, Biophys. Rev. 5 (2013) 187–194.
[50] A.C. Miklos, C. Li, N.G. Sharaf, G.J. Pielak, Volume exclusion and soft interaction effects on protein stability under crowded conditions, Biochemistry 49 (2010) 6984–6991.
[51] J. Wei, J. Dobnikar, T. Curk, F. Song, The effect of attractive interactions and macromolecular crowding on crystallins association, PLoS One 11 (2016), e0151159.
[52] B.T. Edmonds, J. Wyckoff, Y.G. Yeung, Y. Wang, E.R. Stanley, J. Jones, et al., Elongation factor-1 alpha is an overexpressed actin binding protein in metastatic rat mammary adenocarcinoma, J. Cell Sci. 109 (1996) 2705–2714.
[53] B.P. De, S. Gupta, H. Zhao, J.A. Drazba, A.K. Banerjee, Specific interaction in vitro and in vivo of glyceraldehyde-3-phosphate dehydrogenase and LA protein with cis-acting RNAs of human parainfluenza virus type 3, J. Biol. Chem. 271 (1996) 24728–24,735.
[54] M. Sioud, L. Jespersen, Enhancement of hammerhead ribozyme catalysis by glyceraldehyde-3-phosphate dehydrogenase, J. Mol. Biol. 257 (1996) 775–789.
[55] X. Wu, Y. Zhou, K. Zhang, Q. Liu, D. Guo, Isoform-specific interaction of pyruvate kinase with hepatitis C virus NS5B, FEBS Lett. 582 (2008) 2155–2160.
[56] D. Simsek, G.C. Tiu, R.A. Flynn, G.W. Byeon, K. Leppek, A.F. Xu, et al., The mammalian Ribo-interactome reveals ribosome functional diversity and heterogeneity, Cell 169 (2017) (1051–1065.e1018).
[57] S.K. Mukherjee, S. Gautam, S. Biswas, J. Kundu, P.K. Chowdhury, Do macromolecular crowding agents exert only an excluded volume effect? A protein solvation study, J. Phys. Chem. B 119 (2015) 14145–14,156.
[58] L. Bekale, D. Agudelo, H.A. Tajmir-Riahi, The role of polymer size and hydrophobic end-group in PEG–protein interaction, Colloids Surf. B: Biointerfaces 130 (2015) 141–148.
[59] R. Krishnan, M.R. Blanco, M.L. Kahlscheuer, J. Abelson, C. Guthrie, N.G. Walter, Biased Brownian ratcheting leads to pre-mRNA remodeling and capture prior to first-step splicing, Nat. Struct. Mol. Biol. 20 (2013) 1450–1457.
[60] S. Pitchiaya, L.A. Heinicke, T.C. Custer, N.G. Walter, Single molecule fluorescence approaches shed light on intracellular RNAs, Chem. Rev. 114 (2014) 3224–3265.
[61] R. Russell, RNA misfolding and the action of chaperones, Front. Biosci. 13 (2008) 1–20.
[62] E.C. Ferguson, J.C. Rathmell, New roles for pyruvate kinase M2: working out the Warburg effect, Trends Biochem. Sci. 33 (2008) 359–362.
[63] A. Castello, B. Fischer, C.K. Frese, R. Horos, A.M. Alleaume, S. Foehr, et al., Comprehensive identification of RNA-binding domains in human cells, Mol. Cell 63 (2016) 696–710.
[64] B.E. Docter, S. Horowitz, M.J. Gray, U. Jakob, J.C. Bardwell, Do nucleic acids moonlight as molecular chaperones? Nucleic Acids Res. 44 (2016) 4835–4845.
[65] M.J. Gray, W.Y. Wholey, N.O. Wagner, C.M. Cremers, A. Mueller-Schickert, N.T. Hock, et al., Polyphosphate is a primordial chaperone, Mol. Cell 53 (2014) 689–699.
[66] A. Patel, L. Malinovska, S. Saha, J. Wang, S. Alberti, Y. Krishnan, et al., ATP as a biological hydrotrope, Science 356 (2017) 753–756.
[67] N.G. Walter, Probing RNA structural dynamics and function by fluorescence resonance energy transfer (FRET), Curr Protoc Nucleic Acid Chem Chapter 11.10 (2003) 11.10.1–11.10.23.
[68] N.G. Walter, K.J. Hampel, K.M. Brown, J.M. Burke, Tertiary structure formation in the hairpin ribozyme monitored by fluorescence resonance energy transfer, EMBO J. 17 (1998) 2378–2391.

[69] K.C. Suddala, J. Wang, Q. Hou, N.G. Walter, Mg2+ shifts ligand-mediated folding of a riboswitch from induced-fit to conformational selection, J. Am. Chem. Soc. 137 (2015) 14075–14083.
[70] P. Gonzalez-Tello, F. Camacho, G. Blazquez, Density and viscosity of concentrated aqueous solutions of polyethylene glycol, J. Chem. Eng. Data 39 (1994) 611–614.
[71] P. Thiyagarajan, D.J. Chaiko, R.P. Hjelm, A neutron scattering study of poly(ethylene glycol) in electrolyte solutions, Macromolecules 28 (1995) 7730–7736.
[72] P.B. Rupert, A.R. Ferre-D'Amare, Crystal structure of a hairpin ribozyme-inhibitor complex with implications for catalysis, Nature 410 (2001) 780–786.
[73] S.E. McDowell, J.M. Jun, N.G. Walter, Long-range tertiary interactions in single hammerhead ribozymes bias motional sampling toward catalytically active conformations, RNA 16 (2010) 2414–2426.

Supplementary Information:

Soft interactions with model crowders and non-canonical interactions with cellular proteins stabilize RNA folding

May Daher[1,2,†], Julia R. Widom[1,2], Wendy Tay[1,3] and Nils G. Walter*[1,2]

1 - Single Molecule Analysis Group, Department of Chemistry

2 - Center for RNA Biomedicine

3 - Program in Chemical Biology, University of Michigan, Ann Arbor, MI 48109-1055, USA

†Present Address: Department of Chemistry and Biochemistry, University of Detroit Mercy, Detroit, MI 48221-3038

Correspondence to Nils G. Walter: nwalter@umich.edu

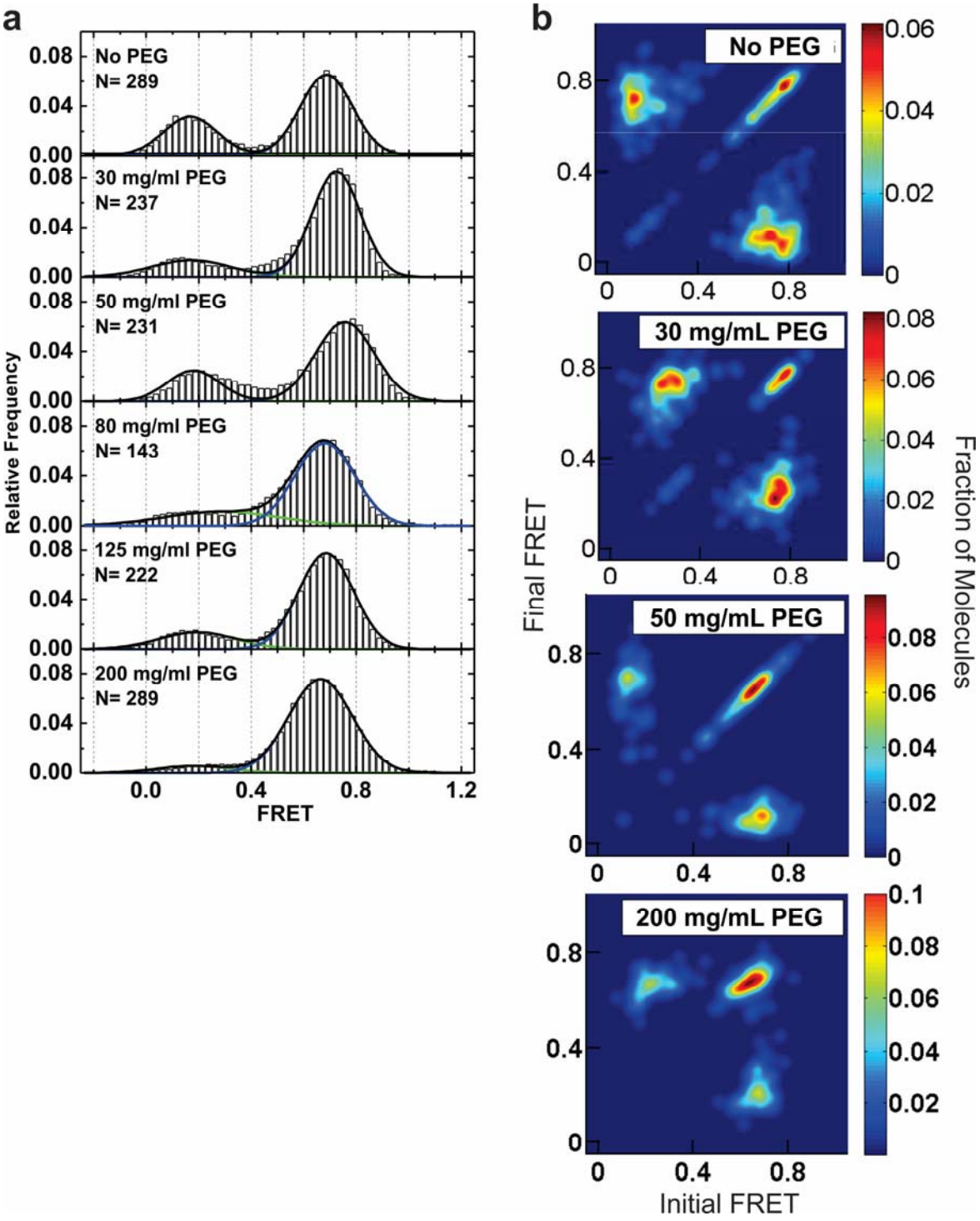

Supplementary Fig. S1. PEG stabilizes the stably docked conformation of the hairpin ribozyme. (**a**) FRET histograms for over N single molecule time trajectories each are shown at different PEG concentrations. (**b**) Transition occupancy density plots (TODPs) illustrate the fraction of hairpin ribozyme molecules that undergo a transition from a given initial FRET state to a given final FRET state. Molecules that are static, either docked or undocked, are revealed on the diagonal at the position of the occupied FRET state.

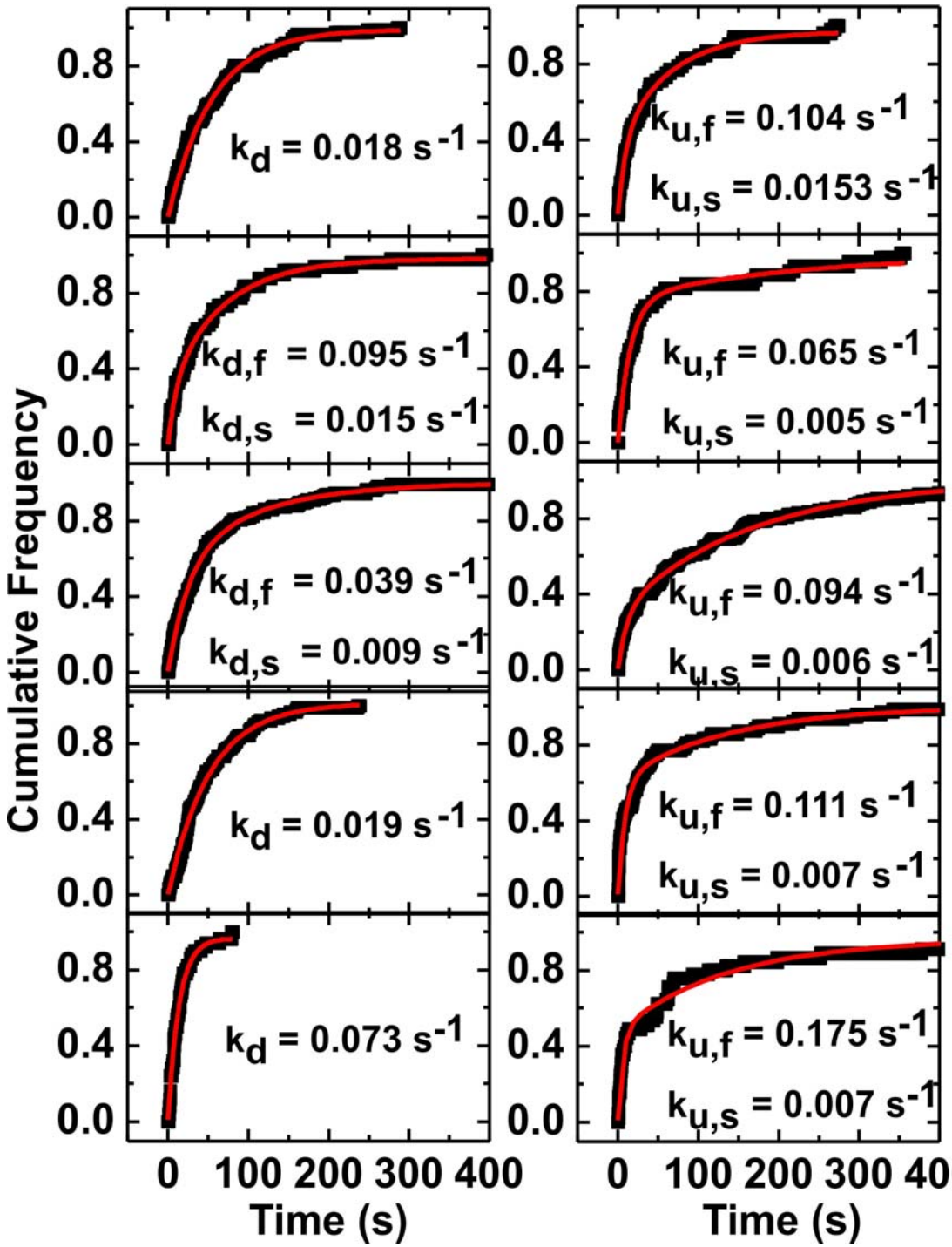

Supplementary Fig. S2. The dynamic population reveals heterogeneities in the presence of PEG. Dwell time distributions were plotted for the dynamic docked and undocked populations in the presence of 0, 30, 50, 80 and 200 mg/mL of PEG (top to bottom). The distributions were fitted with single– or double-exponentials to obtain the docking and undocking rates constant k_d and k_u of the fast (f) and slow (s) molecular sub-populations, respectively, as described [1, 2]. The fitting was performed using Microcal Origin software.

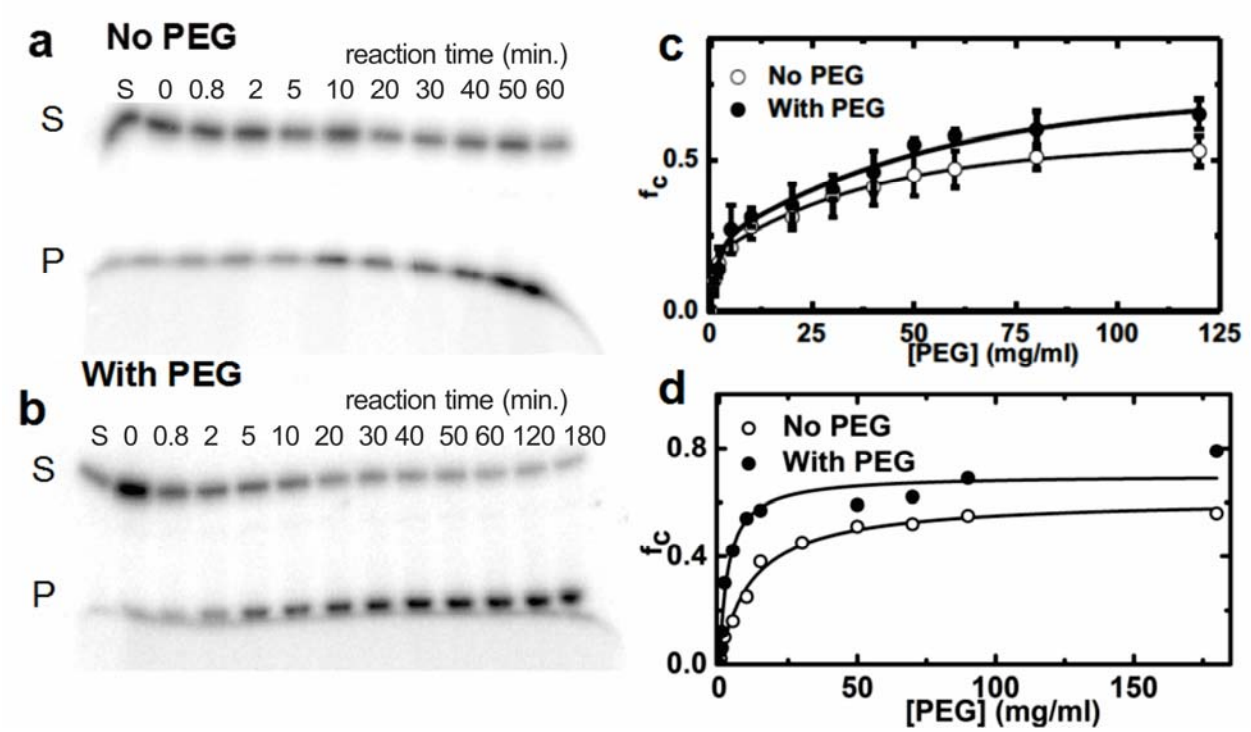

Supplementary Fig. S3. The presence of PEG leads to enhanced ribozyme cleavage. (**a**) Gel electrophoretic analysis of the fraction of intact substrate (S) and cleaved product (P) as a function of time (0−180 min) for the hairpin ribozyme in the absence of PEG. (**b**) Gel electrophoretic analysis of the fraction of intact substrate (S) and cleaved product (P) as a function of time (0−180 min) in the presence of 200 mg/mL of PEG. (**c**) and (**d**) Fraction of cleaved product, $f_{cleaved}$, as a function of time in standard reaction buffer with either 12 mM $MgCl_2$ or 5 mM $MgCl_2$ at room temperature. In the presence of PEG, the ribozyme generates significantly more product, especially at low Mg^{2+} concentration, leading to double-exponential fits as described [1, 2].

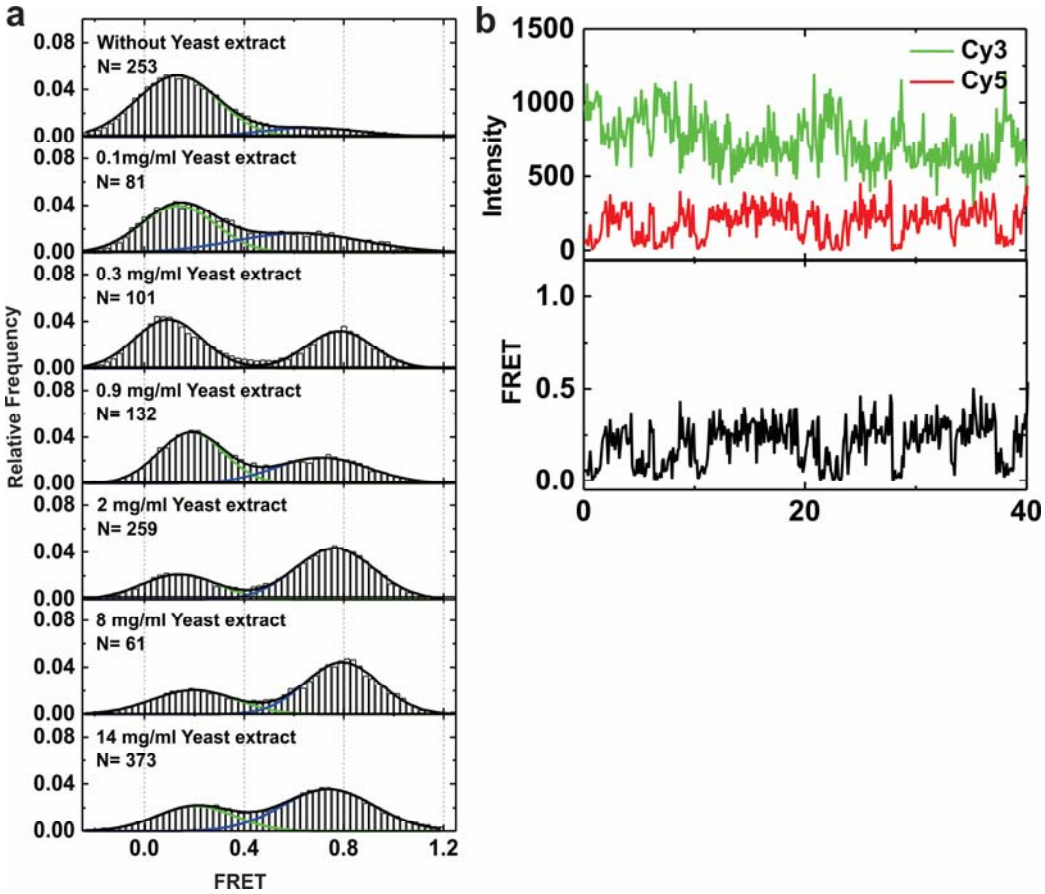

Supplementary Fig. S4. The hairpin ribozyme folds at very low concentrations of yeast WCE. (**a**) smFRET histograms built from N single molecule time trajectories each, at different yeast extract concentrations. The results reveal two main FRET states, low-FRET (undocked) and high-FRET (docked). The data were fitted with Gaussian distributions (green and blue lines, respectively). (**b**) Representative donor, acceptor (top panel), and FRET trajectories (bottom panel) reveal a small fraction of molecules with fluctuations within the low-FRET envelope.

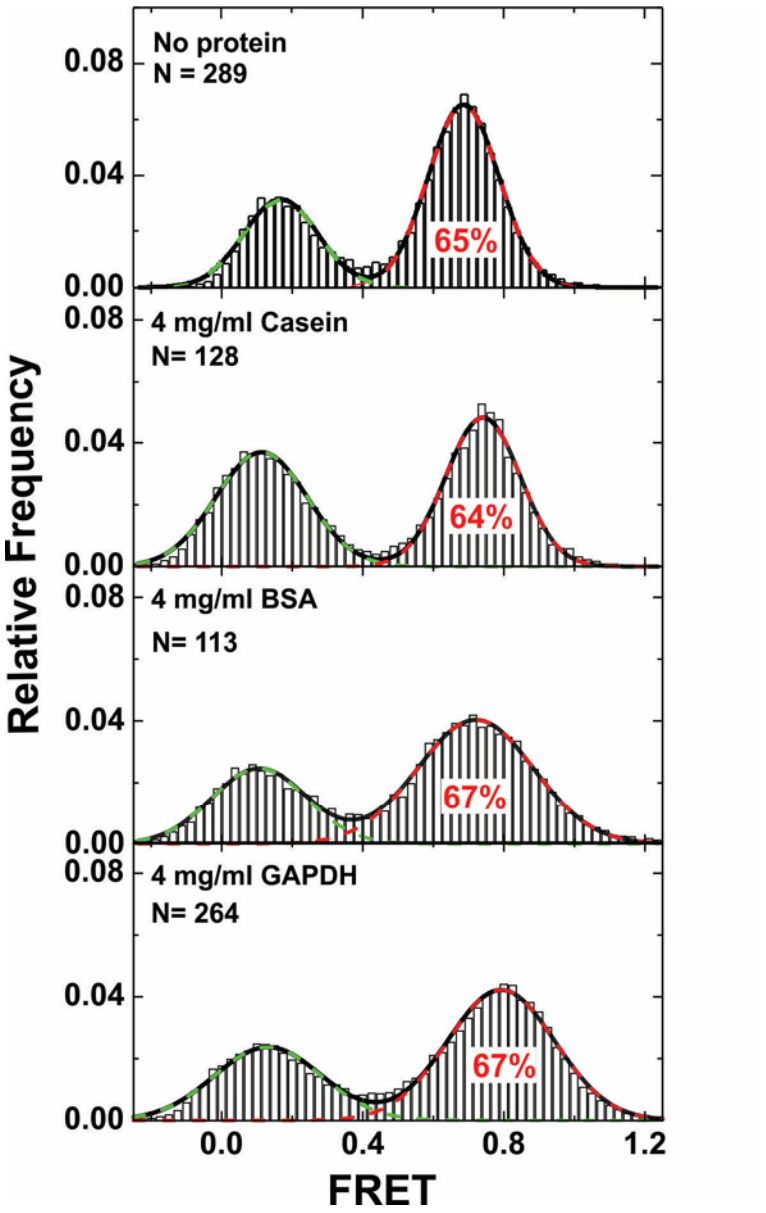

Supplementary fig. S5. Changes to FRET histograms upon addition of high concentrations of individual proteins in standard buffer. These proteins, which were not shown to bind to the hairpin ribozyme, do not affect folding even at much higher concentrations than yeast extract.

Supplementary Table S1. Parameters obtained from excluded volume, native state binding and hybrid models. All fits were subject to the constraint that $r_{undock} \geq r_{dock}$. We note that the values of $K_{D,undock}$ and $K_{D,dock}$ are poorly defined for the 12 mM Mg^{2+} hybrid model due to the lack of data at PEG concentrations below saturation.

	1 mM Mg^{2+}			12 mM Mg^{2+}		
model	EV	NSB	hybrid	EV	NSB	hybrid
r_{undock} (Å)	31.2	N/A	26.3	28.5	N/A	27.7
$K_{D,undock}$ (mg/mL)	N/A	83	83	N/A	146	7
$K_{D,dock}$ (mg/mL)	N/A	250	250	N/A	338	10
R^2	0.20	0.93	0.93	0.32	0.52	0.77

Supplementary Table 2. A selection of the yeast proteins that were enriched upon pull-down with the hairpin ribozyme.

Gene Name	Full Name	Function
HSC82	82 kDa Heat shock cognate protein	Molecular chaperone and stress response
SSB1	Stress-seventy subfamily B, HSP70 family	Cotranslational folding of newly synthesized proteins
VMA2	Subunit of vacuolar membrane ATPase	Hydrolase activity, catalyzing transmembrane movement of substances
PK	Pyruvate kinase	Glycolysis
ALD	Aldehyde dehydrogenase	Performs the conversion of acetaldehyde to acetate
SHM1	Serine hydroxymethyltransferase	Tetrahydrofolate interconversion pathway
TBB	Tubulin beta chain	Microtubules stability
LYS9	Saccharopine dehydrogenase	Aminoacid biosynthesis; lysine biosynthesis
PGK	Phosphoglycerate kinase	Glycolysis

References

[1] D. Rueda, G. Bokinsky, M.M. Rhodes, M.J. Rust, X. Zhuang, N.G. Walter. Single-molecule enzymology of RNA: essential functional groups impact catalysis from a distance. Proc. Natl. Acad. Sci. USA 101 (2004) 10066-71.

[2] X. Zhuang, H. Kim, M.J. Pereira, H.P. Babcock, N.G. Walter, S. Chu. Correlating structural dynamics and function in single ribozyme molecules. Science 296 (2002) 1473-6.